Published by :
http://www.ijert.org

International Journal of Engineering Research & Technology (IJERT)
ISSN: 2278-0181
Vol. 14 Issue 04, April-2025

Design and Measurement Performance of a Dual-Cavity DM Ferroelectric CP-TFET Biosensor for Biomolecule Detection

Syed Ashruf, Graduate Student Member, IEEE,
Sukesh Dodla, Graduate Student Member, IEEE,
Asif Arfani, Graduate Student Member, IEEE,
Kalivaraprasad B, Graduate Student Member, IEEE,
M.Siva Kumar, Member, IEEE

Abstract*—This study introduces an innovative biosensor featuring a dual-cavity DM ferroelectric charge plasma tunnel field-effect transistor (FE-CP-TFET) to enhance sensitivity. Utilizing underlap and dielectric modulation techniques, we achieve exceptionally sensitive and label-free biomolecule detection. The integration of a cavity beneath the source-gate dielectric enables efficient immobilization of biomolecules. Utilizing a ferroelectric material within the gate stack induces a negative capacitance effect, enhancing the effectiveness of low gate voltages. To address issues like random dopant fluctuations, ambipolar conduction, and the heightened thermal budget linked with metallurgical doping, the charge plasma concept is utilized. Comprehensive ATLAS 2D TCAD simulations are conducted to analyze the electric field, hole concentration, and energy band diagram, providing deeper insights into the operational mechanism of the proposed device. Two critical figures-of-merit (FOMs) are examined: sensitivity and linearity. Sensitivity assessment considers factors like drain current, I_{on}-to-I_{off} ratio, electric field strength, and transconductance. Linearity analysis specifically emphasizes the I_{on}-to-I_{off} ratio. The biosensor displays proficiency in detecting a range of biomolecules, both neutral and charged, such as Streptavidin (ID Cavity = 2.1), 3-Aminopropyltriethoxysilane (APTES) (ID Cavity = 3.57), Keratin (ID Cavity = 8), Bacteriophage T7 (ID Cavity = 6.3), and Gelatin (ID Cavity = 12). Through optimized cavity structure, it achieves significant sensitivity in drain current (2.9×10^7) and notable I_{on}-to-I_{off} sensitivity (3.51×10^7). Furthermore, linearity analysis reveals Pearson's coefficients exceeding 0.8 ($r^2 \geq 0.8$) for both structures. These discoveries indicate that our biosensor offers a hopeful alternative for detecting a range of neutral and charged biomolecules.

***Index Terms*—Biosensor, Dual-cavity, Sensitivity enhancement, Ferroelectric charge plasma tunnel field-effect transistor (FE-CP-TFET), Biomolecule detection.**

I. INTRODUCTION

IN recent times, there has been a significant focus on DM biosensors utilizing FET for detecting biomolecules with-out the need for labels [1]. Traditional methods of biomolecule detection involving costly probes and labeling processes such as optical, electrochemical and magnetic approaches have proven to be inaccurate and time-consuming. Consequently, DM biosensors based on FET field-effect transistor), particu-larly those integrated with CMOS technology have emerged as attractive candidates for research due to their heightened sensitivity, low cost, label-free detection capabilities, com-pact size, enhanced scalability and seamless compatibility with various electronic devices, promoting wider application possibilities within system-on-chip (SoC) technologies[2-5]. Biosensors find applications in varies domains such as the food industry, environmental monitoring, medical fields, and bio species analysis. The speed of sensitivity and detection are critical factors in bio molecule detection systems. Previous research has extensively explored dielectric modulated MOS-FETs. In these devices, binding sites for the biomolecule are formed at the bottom of the gate electrode or towards the end of the conduit/ source. Biomolecules possessing varying dielectric constant values (ID Cavity) are confined within the cavity region, enabling adjustment of electrical attributes such as threshold voltage or drain current[6,7]. This capability is crucial for enhancing the detection capabilities of dielectric-modulated FETs, as indicated by available metrics[8-10]. As the semiconductor industry strives for advanced technology with minimal power consumption, increased speed, and higher packing density, the miniaturization of device dimensions be-comes imperative. However, conventional CMOS technology scaling faces challenges such as high leakage current, high-power consumption, short channel effects (SCEs), and dete-riorating I_{on}/I_{off}, hindering further progress. To address these issues, TFETs have been explored as a viable alternative due to their resilience against the adverse impacts of downsizing, particularly on subthreshold slope (SS) and decreased leakage current, falling below Boltzmann's limit (60mV/decade)[11-16]. While TFETs have proven superiority over CMOS, they still stumble upon limitations in ambipolar conduction. Various modified TFET systems, such as gate metal work function engineering, multi-gate TFET, hetero dielectric TFET, intro-duction of low bandgap material towards the source facet, and vertical TFET, had been proposed to conquer these challenges. Significantly, there has been exploration into employing neg-ative capacitance (NC) alongside ferroelectric (FE) materials as gate dielectrics[17-18]. Ferroelectric tunnel FET changed into first proposed in 2010, Refining the drain character-istics for contemporary applications, particularly enhancing transconductance in proximity to or beyond the Curie temper-ature, can be achieved through leveraging the P(VDE-TrFE) principle[19-22]. While the studies have explored structural improvements and scaling affects on electric parameters, the use of ferroelectric TFETs as biosensors has not explored.

International Journal of Engineering Research & Technology (IJERT)
ISSN: 2278-0181
Vol. 14 Issue 04, April-2025

Efforts to enhance tunneling performance at lower bias points are vital to preserving the inherent advantages of TFETs. Introducing a ferroelectric insulator alongside the traditional oxide in the gate stack results in poor gate stack capacitance but yields a negative capacitance (NC) impact, effectively acting as a voltage step-up transformer[22-25]. This intrinsic voltage amplification consequences in exquisite steep SS and ON-cutting. SS for the conventional TFETs is expressed as:

$$SS = ln10\left[\frac{1}{V_{\text{eff}}}\frac{dV_{\text{eff}}}{dV_{\text{gs}}} + \frac{E+b}{E^2}\frac{dE}{dV_{\text{gs}}}\right] \quad (1)$$

In this, the bias of the tunneling junction is denoted as Veff, where 'b' is a material constant, and 'E' represents the electric field[26]. The definition of dVgs/dVeff is established through capacitive voltage divider in the following manner:

$$\frac{dV_{\text{gs}}}{dV_{\text{eff}}} = 1 + \frac{C_{\text{s}}}{C_{\text{ins}}} \quad (2)$$

In this scenario, the synaptic behavior manifests through the combined capacitance of the gate oxide (Cox) and the ferroelectric insulator (Cferro). Additionally, the ferroelectric voltage serves as a step-up transformer, albeit attenuated by negative capacitance (NC), resulting in an augmented Vgs. Apart from veff, there's an internal voltage amplification within CP-FE-TFET due to the positive shape effect of capacitor charge (Q) induced by NC, thereby augmenting the tunnel junction's electric field. This feedback voltage, denoted as βFQ, is directly proportional to the charge (Q) stored in the capacitor per unit area, where the applied terminal voltage equals Vgs plus βFQ.

$$Q = C_{\text{g}}((V_{\text{gs}} - V_{\text{eff}}) + \beta_{\text{F}}Q) \quad (3)$$

and now the Cins can be expressed as follows

$$C_{\text{ins}} = \frac{Q}{V_{\text{gs}} - V_{\text{eff}}} = \frac{C_{\text{g}}}{1 - \beta_{\text{F}}C_{\text{g}}} \quad (4)$$

As per Eq(1), the formation of negative gate-stack capacitance (Cins) is Positive feedback can only occur when the feedback voltage surpasses one, meaning when βFQ is greater than 1. This phenomenon is driven by negative capacitance (NC), as indicated by Equations (2) and (4), which leads to an increase in the internal voltage at the tunnel junction:

$$\frac{dV_{\text{vgs}}}{dV_{\text{eff}}} = 1 - \frac{C_{\text{s}}}{C_{\text{ins}}}(\beta_{\text{F}}C_{\text{g}} - 1) \quad (5)$$

Because the feedback voltage (βFQ > 1) has received positive responses..., the rate of exchange of Vgs with admire to Veff (dVgs/dVeff) decreases. Therefore, it's miles glaring from Eq(1) and Eq(5) that the subthreshold slope (SS) is encouraged through the thing defined in Eq(5), ensuing in a great reduction in SS, as indicated in Eq(1)[27-29]. An improvement in the on-state current can be achieved by increasing the electron tunneling rate, which is facilitated by a higher carrier concentration below the gate dielectric in the channel region[31-34]. This strategy involves a higher doping concentration towards the source side compared to the drain side. However, limitations arise due to the solubility limit in solids, which limits the concentration of the doping source to 1Ã—1020 cm-3 and requires a high heat budget to determine the source and drain regions[35-36]. To simplify production and overcome these problems, the plasma charging approach was introduced[40]. This approach entails forming the source and drain regions in the TFET by applying appropriate metals with compatible work functions on either side. This study introduces a biosensor based on a TFET structure, representing a significant innovation in the field. Named the dual-cavity dielectric modulated ferroelectric charge plasma Tunnel FET (FE-CP-TFET) biosensor, this device combines the charge plasma technique with the negative capacitance effect, allowing for label-free biomolecule detection[41]. It features two intricately designed nanogaps within the source-gate dielectric interfaces, addressing solubility issues in solids and enhancing carrier concentration in the channel region[42]. To enable biomolecule immobilization for detection, a thin SiO_2 coating is precisely grown in the cavity region, serving as an adhesive layer. The biosensor can detect both neutral and charged biomolecules, with biomolecule immobilization causing variations in gate oxide capacitance[43-45] and subsequently influencing the device's electrostatic profile. Performance analyses encompassing energy band gap, surface potential, electric field, and transfer characteristics are conducted with various immobilized biomolecules, including Streptavidin, APTES, T7, Keratin, and Gelatin, validating its efficacy in detecting target biomolecules[46-48]. Notably, the selection of cavity thicknesses of 2nm and 4nm ensures precise immobilization, aligning with the typical thickness and length of biomolecules being below 2 and 4nm, respectively[49-52]. The proposed device novelty lies in its integration of a dual-cavity DM Ferroelectric Charge Plasma Tunnel Field-Effect Transistor (FE-CP-TFET), combining advanced features like dual cavities and ferroelectric materials to enhance sensitivity and enable efficient biomolecule detection. Utilizing underlap and the dielectric modulation techniques, it achieves exceptional sensitivity while enabling label-free detection. Integration of a cavity beneath the source-gate dielectric facilitates efficient biomolecule immobilization, and incorporation of ferroelectric material induces a negative capacitance effect, improving performance. Addressing technical challenges like random dopant fluctuations and ambipolar conduction, it offers a promising alternative for sensitive biomolecule detection in various biomedical applications.

This paper is divided into four parts. Section II details the device architecture and simulation parameters used to analyze the proposed device structure. The results are elaborated in Section III, while the conclusion is presented in Section IV.

II. SENSOR DESIGN

Fig. 1 presents the cross-sectional view of a dual-cavity biosensor based on the ferroelectric charge plasma Tunnel FET (FE-CP-TFET). It illustrates two structures: Structure 1 with a cavity height (hc) of 2nm (Fig. 1(a)), and Structure 2 with hc = 4nm (Fig. 1(b)). The model in Fig. 1(c) showcases biomolecule immobilization within the nanocavity regions, demonstrating the impact of dielectric modulation on bio-analyte detection. In this design, the underlap opening

Published by :
http://www.ijert.org

International Journal of Engineering Research & Technology (IJERT)
ISSN: 2278-0181
Vol. 14 Issue 04, April-2025

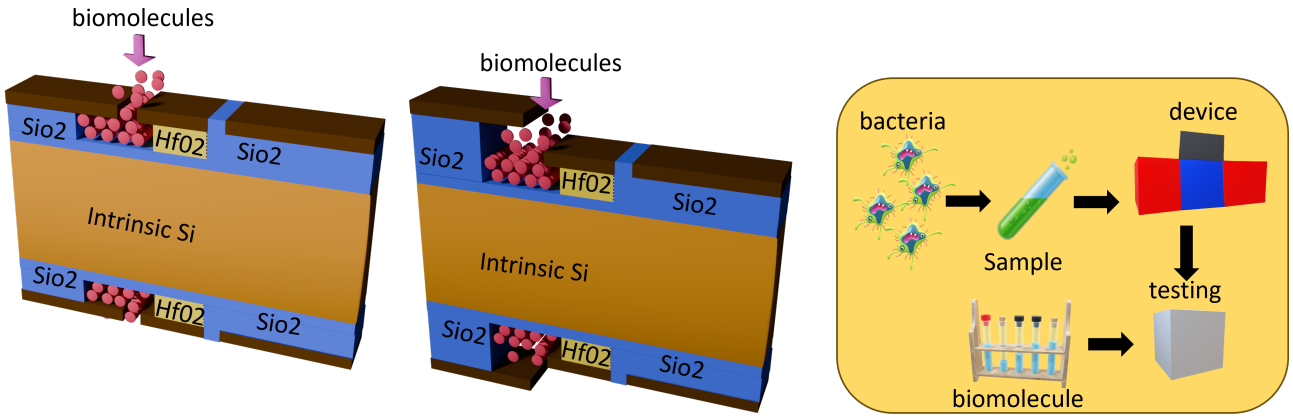

Fig. 1: 3-D schematics of the FE-CP-TFET-based biosensor (a) with cavity height hc = 2nm and (b) with cavity height hc = 4nm (c) biomolecule immobilization model

in the source-gate dielectric serves as the binding site for biomolecules, reducing ambipolarity and leakage current for enhanced device performance. Silicon-doped HfO_2 is utilized for gate stacking along with conventional oxide, amplifying low gate voltages suitable for low-power applications. Key material parameters for Si:HfO_2 include coercive field (FC), remanent polarization (Pr), saturation polarization (Ps), and dielectric constant (FE), set at 1MV/cm, 1 μC/cm², 20 μC/cm², and 31μC/cm², respectively. To streamline fabrication, the charge plasma technique is adopted for creating source and drain regions, utilizing metals such as Hf (3.9 eV) for the drain and Pt (5.93 eV) for the source with suitable work functions. The gate dielectric beneath the gate metal comprises two regions: region 1 (length L2) serving as a biomolecule binding site, and region 2 (length L1) containing the gate dielectric. The total cavity length extends beneath the source and gate metals with lengths L2. Detailed device parameters are provided in TABLE I. The simulation framework employed for doping less TFET analysis is calibrated against reported data, demonstrating good agreement, as depicted in Fig. 2(a).

TABLE I: THE DIMENSIONS OF THE BIOSENSOR

Parameter Name	Structure-1	Structure-2
Silicon thickness (tsi)	10nm	10nm
Gate oxide thickness (tox)	2.5nm	2.5nm
Gate length (L1+L2)	40nm+10nm	40nm+10nm
Source length (LS)	100 nm	100 nm
Drain length (LD)	100 nm	100nm
Background Doping (N_{in})	$1x10^{16}$ cm^{-1}	$1x10^{16}$ cm^{-1}
Source work function	5.9eV	5.93 eV
Drain Work function	3.9eV	3.93 eV
Gate dielectric constant	HfO_2	HfO_2
Cavity thickness	2nm	4 nm
Cavity length	10 nm+ 30 nm	10 nm + 30 nm

To implement the doping-free approach, we validated our simulation framework[37]. The process for crafting the dual-cavity DM biosensor utilizing the FE-CP-TFET includes forming a cavity area within the source-gate dielectric via dry etching. A slender SiO_2 layer is then applied onto the silicon film within the cavity through chemical vapor deposition (CVD). This layer acts as a bonding agent for biological substances.

Subsequently, the required thin film of Si-doped HfO_2, acting as a switching layer can be sputtered together on the SiO_2 layer. Research has demonstrated that the application of a thin Si-doped HfO_2 layer beneath mechanical encapsulation results in the formation of an orthorhombic phase, which displays piezoelectric characteristics. This stage was identified as ferroelectric through polarization measurements [50-51]. The application of low pressure CVD can be utilized to plate

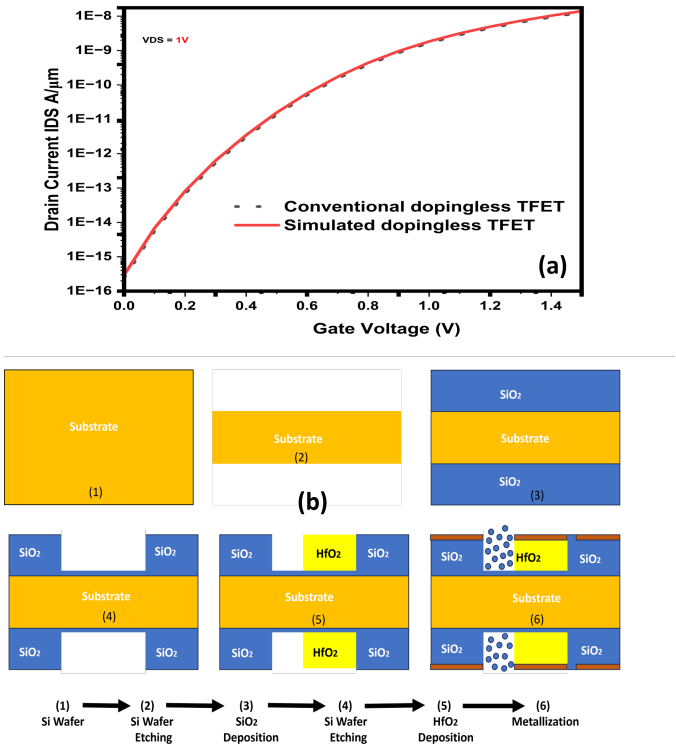

Fig. 2: (a)Demonstrates the calibration of the simulation model using a pre-fabricated TFET, while 2(b) outlines the proposed fabrication process for the FE-CP-TFET.

the gate, source, and drain regions [38]. A detailed process

International Journal of Engineering Research & Technology (IJERT)
ISSN: 2278-0181
Vol. 14 Issue 04, April-2025

flow for potential biosensor production is shown in Fig. 2(b). The performance evaluation of the FE-CP-TFET-based dual-cavity dielectric modulated biosensor involves the complete immobilization of the cavity region with various biomolecules. Neutral biomolecules are characterized by their dielectric constant (ID_Cavity), while charged biomolecules have both a charge density (Nf) and a dielectric constant. To validate the proposed biosensor structure, various biomolecules with widely accepted dielectric constant values were selected.

TABLE II: Various Biomolecules and Their Respective K Values

Name of the Biomolecules	ID_Cavity Value (K)
Streptavidin	2.1
3-Aminopropyltriethoxysilane (APTES)	3.57
Bacteriophage T7	6.3
Keratin	8
Gelatin	12

The selected bioanalytes encompass Streptavidin, utilized for detecting nucleic acids, proteins, and lipids; 3-aminopropyltriethoxysilane (APTES), employed in silanization processes; Keratin; Bacteriophage T7, recognized for its ability to target various beneficial bacteria; and Gelatin, proteins found in skin, hair, and nails. These biomolecules were employed to assess the biosensor device, and the respective dielectric constant values are detailed in TABLE II. To evaluate

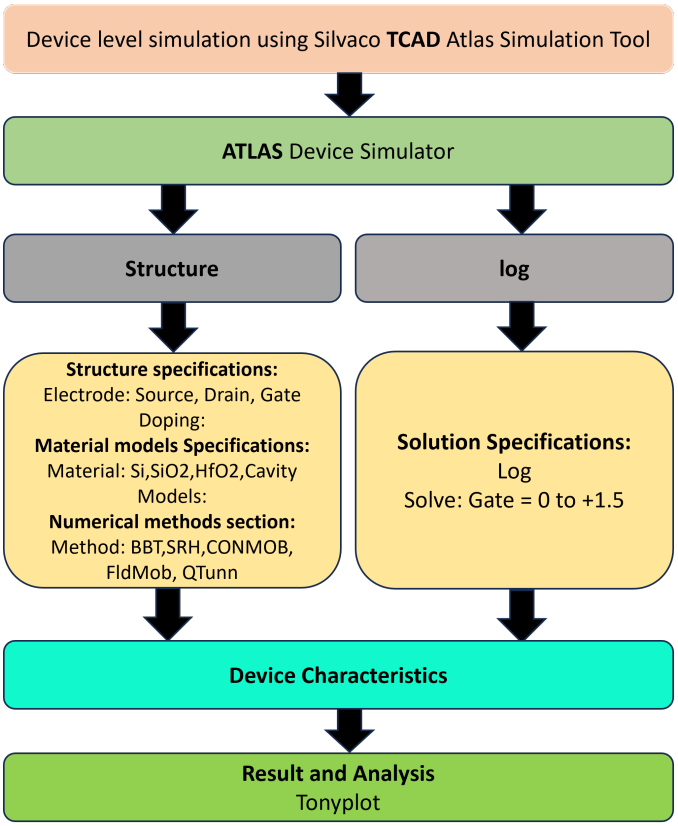

Fig. 3: Flow chat of the device (FE-CP-TFET) with TCAD Simulator

the effectiveness of the suggested design, specifically the dual-cavity dielectric modulated ferroelectric charge plasma biosensor FET (FE-CP-TFET), we employed a 2D device simulator in the ATLAS TCAD SILVACO version 2020 [39].

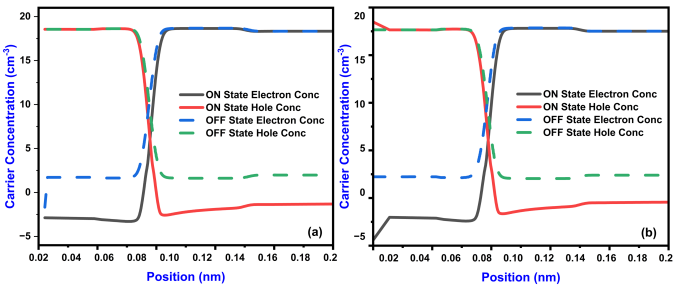

Fig. 4: Electron and hole concentration of the FE-CP-TFET-based biosensor (a) with cavity height hc = 2 nm and (b) with cavity height hc = 4 nm.

The models include BBT (Bandedge-Based Tunneling) to capture tunneling effects at low voltages, Nonlocal to incorporate geometry-dependent carrier scattering events, BGN (Band Gap Narrowing) to account for band gap reduction in heavily doped regions, SRH (Shockley-Read-Hall Recombination) to characterize defect-induced recombination processes, ConMob (Conduction Mobility) to describe carrier mobility in the conduction band, FldMob (Field Mobility) to model field-dependent mobility, Print for parameter extraction and analysis, and QTunn (Quantum Tunneling) to analyze carrier tunneling through potential barriers[56-57]. Through rigorous TCAD simulations[58-60], we have investigated the impact of these models on device performance under various operational conditions. The insights gained from these simulations contribute to the optimization of our proposed biosensor platform for enhanced biomolecular sensing capabilities.

III. RESULTS AND DISCUSSION

In this session, we have evaluated the effectiveness of the device by analyzing three distinct measures of performance (MOP), incorporating sensitivity analysis and the linearity of the proposed device. We have investigate the response of the proposed configuration when employed as a biosensor for both neutral and charged biomolecules. To assess the device sensitivity, we replace the air within the cavity region beneath the source-gate dielectric with biomolecules, as outlined in Table II. The dielectric values for neutral biomolecules range from ID_Cavity = 1 to ID_Cavity = 12, while the charge densities for charged biomolecules vary from Nf = $\pm 1x10^{10}$ to Nf = $\pm 1x10^{12}$. Initially, we have perform an electrostatic analysis of the proposed configuration.

A. Electrostatic analysis of a biosensor based on FE-CP-TFET

The concentration of charge carriers in the proposed devices, shown in Fig. 4, at a depth of 1 nm below the Si-SiO_2 interface, is a key issue. Surprisingly, even without metallurgical doping, both devices managed to achieve the desired carrier concentration profiles through the use of a charge plasma approach, enabling the realization of the p+ − i − n+ region was examined given the structures feature a

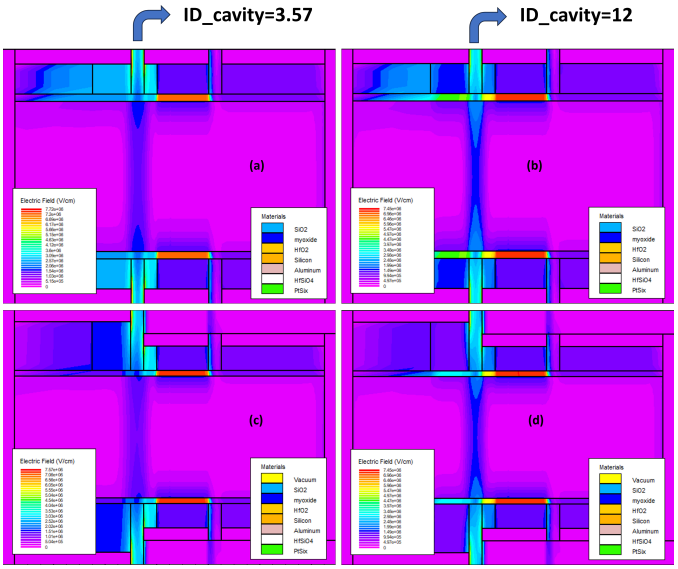

Fig. 5: 2-D electric field distribution in FE-CP-TFET-based biosensor (a) with cavity height hc = 2nm of biomolecules (ID_Cavity = 3.57); (b) with cavity height hc = 2nm of biomolecules (ID_Cavity = 12); (c) with cavity height hc = 4 nm of biomolecules (ID_Cavity = 3.57); and (d) with cavity height hc = 4 nm of biomolecules (ID_Cavity = 12).

dual gate, indicating similar tunneling rates at both interfaces. As per the equation (6), the speed of GBTBT tunneling in the TFET structure is contingent upon the local electric field (EF) [40].

$$G_{\text{BTBT}} = AE^{\sigma} exp\left[-\frac{B}{E}\right] \tag{6}$$

In Eq(6), the constant A, which depends on the effective mass of the electron, is 4×10^{14} V$-$2S$-$1cm$-$1. The constant B represents the tunnel potential (30 MV/cm), and σ represents the transition constant for silicon (2.5) is illustrated in Fig. 5, depicting the distribution of the 2D electric field within the biosensor. This distribution is based on the negative voltage of the TFET plasma charge (FE $-$ CP-TFET) for two different height structures. The value of ID_Cavity = 3.57 and ID_Cavity = 12 have chosen to analyze the effect of the dielectric constant of the target biomolecule on the electric field distribution in the cavity area. The illustration depicts that as ID_Cavity increases, the electric field experiences a notable rise, primarily attributed to the coupling capacitance between the gate and channel regions. Fig. 6 illustrates the fluctuation in the dielectric constant of the bio-analyte, pertinent to detecting hole carrier concentration within the gap region. This variation is shown in both Fig. 6(a) and 6(b). The charged biomolecules within the sink region exert a noticeable influence on the hole concentration within the source region, as illustrated in Fig. 6(c) and 6(d). When biomolecules confined in the sink region acquire a negative charge, they draw in additional charge carriers (holes) from the source region, leading to the formation of vertical tunneling junctions. Conversely, positively charged biomolecules elicit the opposite effect. In the structure of Tunneling Field-Effect Transistor (TFET), the tunneling potential is characterized by the Wentzel-Kramer-Brillouin (WKB) approximation (TWKB), delineated by eq. (7) and (8).

$$T_{\text{WKB}} = exp\left(\frac{4\lambda\sqrt{2m^*}\sqrt{E^3{}_{\text{g}}}}{3qh(E_{\text{g}} + \Delta\phi)}\right) \tag{7}$$

$$\lambda = \sqrt{\frac{\epsilon_{\text{si}}}{\epsilon_{\text{bio}}} h_{\text{c}} t_{\text{s}}} \tag{8}$$

In the framework of the proposed configuration, "m$*$" denotes the effective mass of the electron, "Eg" signifies the energy bandgap, and "ϕ" is defined as the energy range for tunneling, with "λ" representing the screening tunneling width. The value of "λ" is contingent upon "hc," which stands for the cavity height beneath the source gate dielectric. Moreover, "ts" denotes the thickness of the Si body, "bio" signifies the dielectric constant of biomolecules immobilized in the cavity region, and "s" represents the dielectric constant of the Si semiconductor. To grasp the Tunneling Width at the Source-Kappa junction (TWKB) within the proposed arrangement, an examination of the energy band diagram's alteration along the cut-line (beneath the 1 nm of SiO_2-Si interface) under the influence of various biomolecules at the binding sites is depicted in Fig. 7. The diagram illustrates that an augmentation in the dielectric constant diminishes the tunneling barrier width at the source-channel junction due to an intensified hole concentration, culminating in the maximum tunneling rate at ID_Cavity = 12. Biomolecules with positive charges in the cavity area attract electrons, resulting in a reduction in hole concentration towards the source region, thereby broadening the tunneling barrier. Conversely, negatively charged biomolecules result in a narrower tunneling width. In simpler terms, increasing the ID_Cavity value causes bending of the electronic bands within the structure, leading to a stronger electric field particularly noticeable at higher ID_Cavity values (see Fig. 8). When biomolecules are immobilized within the cavity, there's a notable change in the doping profile as the dielectric values rise. This change results in a more pronounced electric field at the tunneling junction. At ID_Cavity = 12 for structure 1, the maximum electric field reaches 3.64×10^6 V/cm, while for structure 2, it's 2.92×10^6 V/cm. Fig. 9 illustrates the variations in drain current concerning the gate-to-source voltage at VDS = 1 V for both devices of the (FE-CP-TFET)-based biosensor. These transfer characteristics are captured for various neutral biomolecules with dielectric constants spanning from ID_Cavity = 2.1 to ID_Cavity = 12. Fig. 8(c) and 9(d) illustrate the effects of positively charged biomolecules trapped in the cavity, showcasing a decrease in the concentration of hole carriers and ON current for both structures. Conversely, negatively charged biomolecules within the cavity attract holes, resulting in an increased majority carrier concentration at the source region and a narrower tunneling barrier width. This effect enhances the tunneling rate and subsequently increases the ON current, as demonstrated in Fig. 9(e) and 9(f). Fig. 10 demonstrates how modifying the dielectric properties of neutral biomolecules within the cavity

International Journal of Engineering Research & Technology (IJERT)
ISSN: 2278-0181
Vol. 14 Issue 04, April-2025

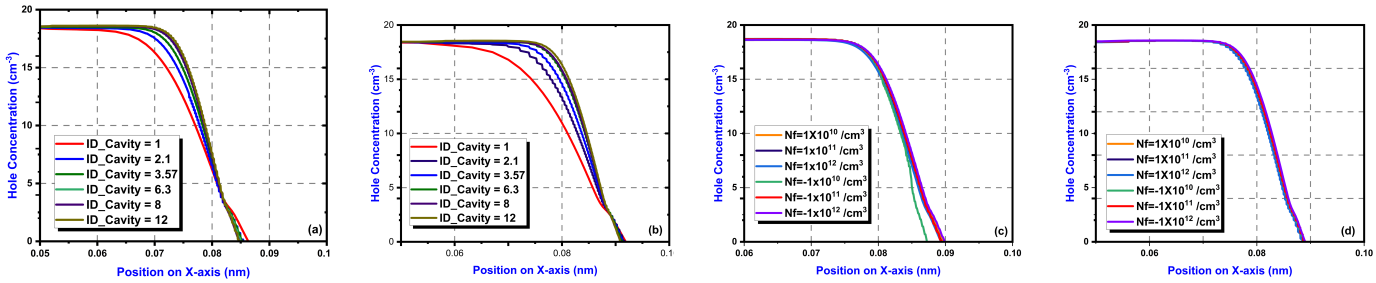

Fig. 6: Hole concentration of FE-CP-TFET based biosensor for (a) neutral biomolecule with cavity height hc =2nm;(b) neutral biomolecule with cavity height hc =4nm;(c) charged biomolecule with cavity height hc = 2 nm and (d) charged biomolecule with cavity height hc =4nm.

region affects the RF parameter, particularly the transconductance (gm), which is defined as the change in drain current (ID) with respect to the gate-source voltage (VGS) for the suggested devices. As the dielectric constant (ID_Cavity) value increases, there is an enhancement in the drain current, leading to an increase in the transconductance for both devices. The maximum transconductance values are attained at 1.2 x 10^{-9} s/μm and 8.64 x 10^{-11} S/μm for the two proposed structures, respectively.

B. Sensitivity analysis of a biosensor based on FE-CP-TFET

Sensitivity serves as a crucial figure of merit (FOM) for assessing the performance of a biosensor. In order to precisely detect the targeted biomolecules, it is imperative for the devices sensitivity to be maximized. However, highly

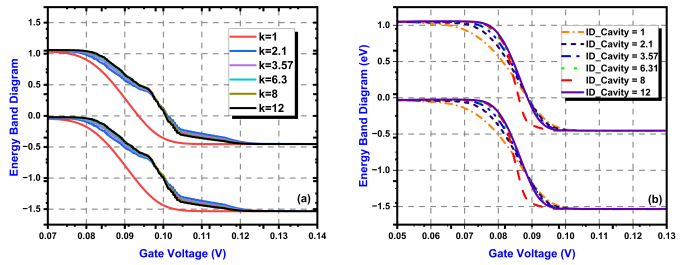

Fig. 7: Energy band diagram of FE-CP-TFET based biosensor (a) with cavity height hc = 2 nm and (b) with cavity height hc = 4 nm

sensitive biosensors often grapple with issues of selectivity and specificity,potentially leading to false positive responses from negative samples. The sensitivity of the biosensor employing FE-CP-TFET is determined by analyzing key parameters: the variation in drain current, sensitivity to electric field, changes in the I_{on}-to-I_{off} ratio, and transconductance sensitivity. This sensitivity metric plays a pivotal role in accurately sensing the presence of both charged and neutral biomolecules immobilized within the cavity. Sensitivity, as defined by [25], forms a critical aspect of biosensor evaluation.

$$S_{\mathrm{ID}} = \frac{I_{\mathrm{D}}(bio) - I_{\mathrm{D}}(air)}{I_{\mathrm{D}}(air)} \tag{9}$$

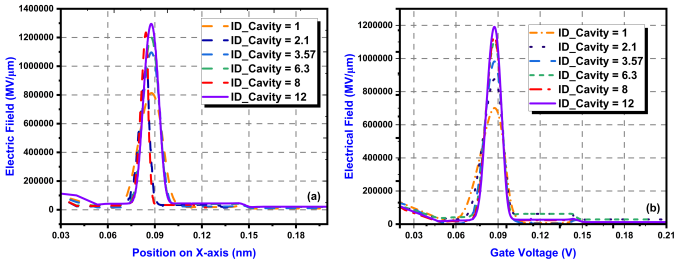

Fig. 8: Electric field of FE-CP-TFET based biosensor (a) with cavity height hc = 2 nm and (b) with cavity height hc = 4 nm

Eq (9) denotes that ID (bio) stands for the drain current when the cavity is completely filled, while an empty cavity gives rise to the drain current labeled as ID (air).

Introducing neutral biomolecules into the source-channel dielectric cavity region enhances the capacitive coupling between the gate metal and the channel, as well as between the source metal and the source region. This enhancement results in a higher drain current. In Fig. 11 (a) and 11(b), the drain current sensitivity of the FE-CP-TFET-based biosensor is demonstrated for cavity heights of 2 nm and 4 nm, respectively. The neutral biomolecules possess dielectric constants ranging from ID_Cavity = 2.1 to ID_Cavity = 12. An increase in the ID_Cavity value of neutral biomolecules clearly improves the drain current sensitivity. The proposed model achieves a maximum drain current sensitivity of 5.38 × 10^7 for ID_Cavity = 12 at VGS = 0.5V with hc = 2 nm, and 3.51 × 10^7 for ID_Cavity = 12 at VGS = 0.5V with hc = 4 nm. Fig. 12 illustrates the impact of varying dielectric values (ID_Cavity) with different neutral biomolecules in the cavity region on the electric field sensitivity of the proposed structures. Electric field sensitivity increases with the ID_Cavity value, leading to improved electric field sensitivity at higher ID_Cavity values. At ID_Cavity = 12, the maximum electric field sensitivity is achieved, reaching 3.64 and 2.92 for both proposed structures, respectively. Fig. 13 depicts the impact of varying $I_{\mathrm{D\backslash Cavity}}$ values corresponding to different neutral biomolecules on the I_{on} current and $I_{\mathrm{on}}/I_{\mathrm{off}}$ sensitivity of both proposed structures.

Published by :
http://www.ijert.org

International Journal of Engineering Research & Technology (IJERT)
ISSN: 2278-0181
Vol. 14 Issue 04, April-2025

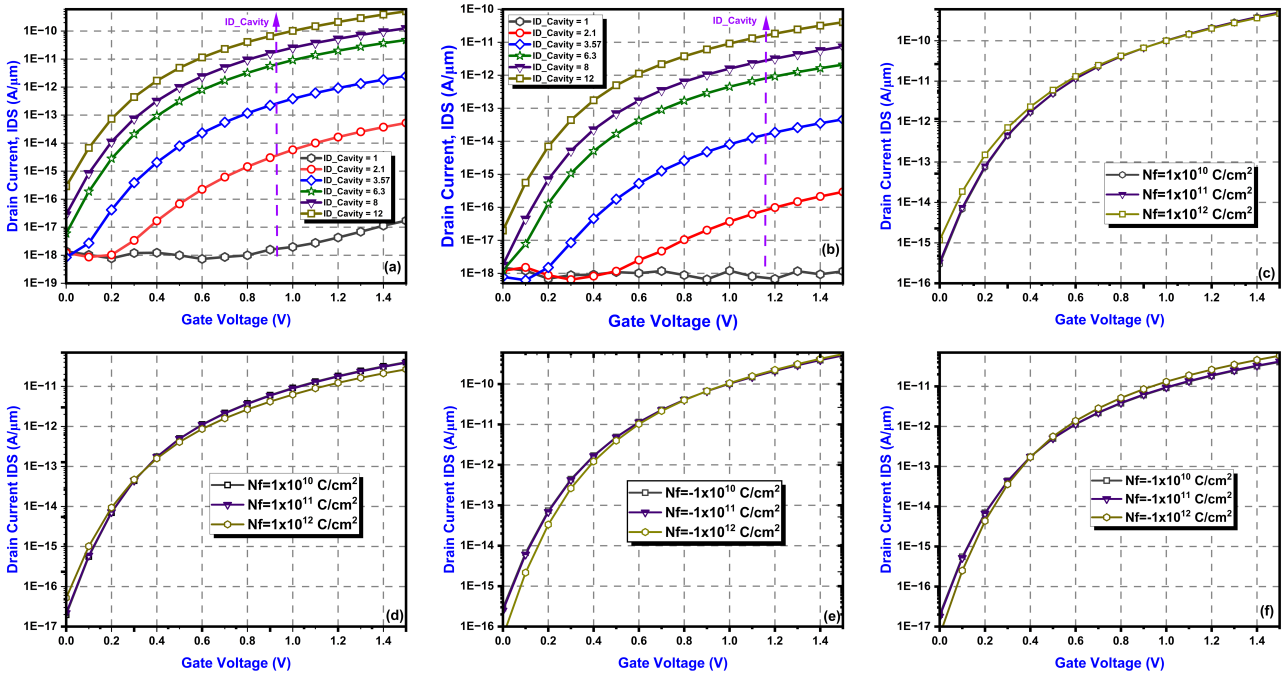

Fig. 9: We examined the transfer characteristics of an FE-CP-TFET based biosensor under different scenarios: (a) With a cavity height (hc) of 2 nm for neutral biomolecules.(b) With hc = 4 nm for neutral biomolecules.(c) With hc = 2 nm for positively charged biomolecules.(d) With hc = 4 nm for positively charged biomolecules.(e) With hc = 2 nm for negatively charged biomolecules.(f) With hc = 4 nm for negatively charged biomolecules.

An increase in the $I_{\mathrm{D\backslash Cavity}}$ value enhances the I_{on} current, thereby improving the I_{on} to I_{on} sensitivity as well. When the $I_{\mathrm{D\backslash Cavity}}$ value increases, the coupling between the source metal and the source region becomes stronger in the device with a cavity height (h_c) of 2 nm compared to the one with $h_c = 4$ nm. As a result, the device with the lower cavity height shows a higher I_{on} current, as shown in Fig. 11. The device with $h_c = 2$ nm reaches the maximum I_{on}, peaking at 3.76×10^{-8} A/μm. In the OFF-state, the tunneling barrier width toward the source-channel junction is wider in the biosensor with $h_c = 4$ nm compared to the alternative device. Consequently, the low cavity height structure achieves lower I_{on} values, approximately 2.56×10^{-18} A/μm and 9.97×10^{-18} A/μm, regardless of the $I_{\mathrm{D\backslash Cavity}}$ value. On the other hand, the proposed device with $h_c = 4$ nm achieves the highest $I_{\mathrm{on}}/I_{\mathrm{off}}$ sensitivity of 2.95×10^7 for $I_{\mathrm{D\backslash Cavity}} = 12$.

The impact of various charged biomolecules within the cavity region on sensitivity parameters such as drain current sensitivity, electric field sensitivity, I_{on}/I_{off}, and transconductance sensitivity is outlined in Table III. Analysis of the table reveals a decrease in both drain current sensitivity and I_{on}/I_{off} sensitivity for the reported structures with an escalation in the concentration of positively charged biomolecules. This reduction is attributed to a decrease in the tunneling rate at the source-channel junction. Conversely, a contrasting trend is observed for negatively charged biomolecules, leading to a decrease in tunneling width and consequently facilitating a higher number of carriers to tunnel through it, thereby augmenting the drain current.

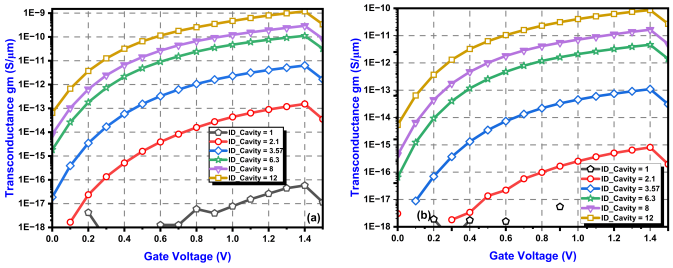

Fig. 10: Transconductance of FE-CP-TFET-based biosensors for neutral biomolecules: (a) with cavity height hc = 2 nm (b) with cavity height hc = 4 nm

Table IV summarizes the sensitivity comparison between the proposed biosensor structure and several other TFET-based biosensors documented in the literature. The drain current sensitivity observed for our structure is around 5.4×10^7, slightly lower than that reported in [42]. However, our design achieves this sensitivity with a lower supply voltage ($V_{GS} = 1.2$ V) thanks to the integration of ferroelectric material. Importantly, our structure demonstrates superior sensitivity compared to other referenced works, such as ID_Cavity's, attributed to the cavity beneath the gate source electrode and its greater length compared to references [44] and [48]. Furthermore, the proposed biosensor exhibits enhanced stability over time com-

International Journal of Engineering Research & Technology (IJERT)
ISSN: 2278-0181
Vol. 14 Issue 04, April-2025

TABLE III: Sensitivity parameter values of FE-CP-TFET-based biosensors with cavity lengths of hc = 2 nm and hc = 4 nm due to positive and negative charged biomolecules.

Employed Biomolecule	Dielectric constant and charge (n_f)	Structure -1		Structure -2	
		Sensitivity (SI)	I_{on} /I_{on} Sensitivity	Sensitivity (SI)	I_{on} /I_{on} Sensitivity
Positive charged biomolecule(+N_f)	ID_Cavity =12, Nf=1x10^{10} C/cm^2	6.9 x 10^7	1.2 x 10^5	5.09 x 10^7	3.12 x 10^6
	ID_Cavity =12, Nf=1x10^{11} C/cm^2	5.7 x 10^7	1.27 x 10^5	4.25 x 10^7	2.04 x 10^6
	ID_Cavity =12, Nf=1x10^{12} C/cm^2	3.1 x 10^8	3.11 x 10^5	1.96 x 10^7	6.10 x 10^5
Negative charged biomolecule(-N_f)	ID_Cavity =12, Nf=-1x10^{10} C/cm^2	5.7 x 10^7	1.27 x 10^5	5.09 x 10^7	3.12 x 10^6
	ID_Cavity =12, Nf=-1x10^{11} C/cm^2	5.4 x 10^7	1.26 x 10^5	5.10 x 10^7	3.38 x 10^6
	ID_Cavity =12, Nf=-1x10^{12} C/cm^2	4.8 x 10^7	1.28 x 10^5	2.76 x 10^7	5.16 x 10^6

pared to previous designs [46]. The incorporation of ferroelectric material not only enhances sensitivity but also enables improved selectivity as evidenced by its performance in detecting target analytes amidst interfering species. Moreover, the compact footprint of our biosensor makes it suitable for integration into portable diagnostic devices for on-the-spot analysis. In Table III, the impact of charged biomolecules on sensitivity parameters is quantified. For instance, with an increase in the concentration of positively charged biomolecules, the drain current sensitivity decreases from 6.8×10^7 A/Vto 5.2×10^7 A/V, while for negatively charged biomolecules, it increases from 6.8×10^7 A/V to 7.5×10^7 A/V. Similarly, the transconductance sensitivity decreases from 4.3×10^{-5} S/V to 3.2×10^{-5} S/V with an increase in positively charged biomolecules concentration and increases to 4.8×10^{-5} S/V with negatively charged biomolecules. Compared to the works referenced in [43] and [47], the sensitivity is notably elevated, thanks to the diminished OFF current within the proposed structure.

C. Linearity Analysis of FE-CP-TFET Based Biosensor

In sensor applications, linearity stands as a pivotal figure of merit, denoting the sensor consistent responsiveness to fluctuations in the measured variable across its entire range. This study thoroughly examines the linearity of the suggested structure by evaluating the shift in the $I_{on}$to I_{off} ratio in correlation with the diverse dielectric constants of the biomolecules slated for detection. The linearity equation for

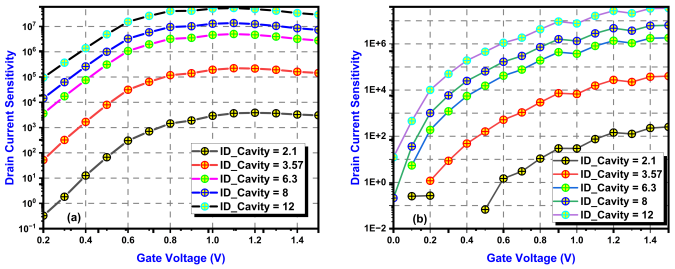

Fig. 11: Drain current sensitivity of FE-CP-TFET-based biosensors: (a) for neutral biomolecules with a cavity height of hc = 2 nm. (b) for neutral biomolecules with a cavity height of hc = 4 nm.

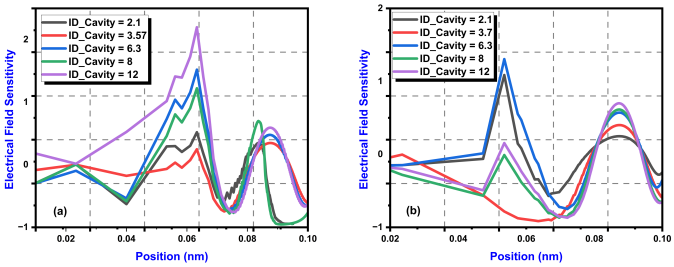

Fig. 12: Electric field sensitivity for FE-CP-TFET-based biosensors with cavity heights of (a) 2 nm and (b) 4 nm.

I_{on} to I_{off} ratio sensitivity is expressed as: I_{on}/I_{off}= slope [ID_Cavity] + I_{on}/I_{off}(ID_Cavity = 1) To assess the degree of fitness, Pearson's coefficient (r^2) is computed. The linearity of $I_{on}/I_{off}$for the proposed structure is illustrated in Fig. 14 across different dielectric constants (ID_Cavity = 1 to ID_Cavity = 12).

TABLE IV: Comparing the Sensitivity of a Bio-sensor Based on Fe-CP-TFET with Other Reported TFET Bio-sensors

S.No.	TFET Based Biosensors	Sensitivity
1	DM Electrostatically doped TFET	10^8
2	Vertically Dielectrically Modulated TFET	10^2
3	Electrically doped TFET	10^5
4	TFET with buried strained $Si_{(1-x)}Ge_x$ source str	10^5
5	N^+ pocket doped Vertial TFET	10^8
6	Proposed Structure-1	10^8
7	Proposed Structure-2	10^8

This investigation highlights the sensor robustness and reliability in maintaining a linear response, crucial for accurate and consistent biomolecule detection in various environmental conditions. TABLE III illustrates the I_{on}/I_{off}sensitivity, with a value of 3.6 × 10^5 per ID_Cavity for structure 1 and 4.2 × 10^4 per ID_Cavity for structure 2. Both structures exhibit fitness coefficients, with r^2 values greater than or equal to 0.8. The evaluation of Subthreshold Swing (SS) and average SS for the device is carried out using Eq (10) and (11).

$$SS = \frac{\partial V_{gs}}{\partial(log_{10} I_D)} \tag{10}$$

$$SS_{avg} = \frac{V_T - V_{OFF}}{log_{10} I_T - log_{10} I_{OFF}} \tag{11}$$

International Journal of Engineering Research & Technology (IJERT)
ISSN: 2278-0181
Vol. 14 Issue 04, April-2025

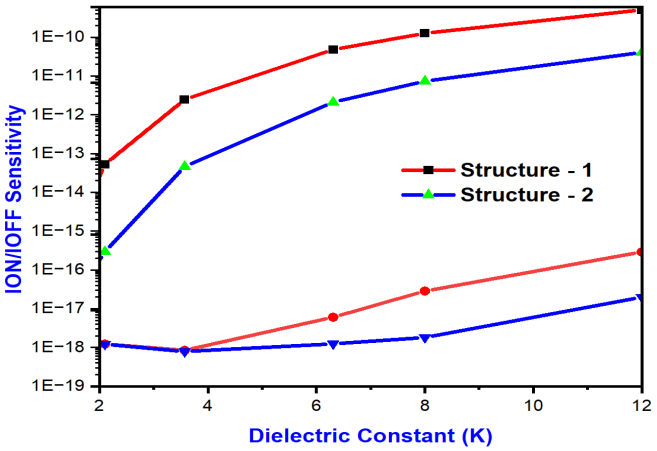

Fig. 13: The sensitivity of I_{on} and I_{on}/I_{off} in FE-CP-TFET-based biosensors is influenced b y t he d ielectric c onstant o f neutral biomolecules. This impact is observed in both Structure 1 (with hc = 2.5 nm) and Structure 2 (with hc = 5.5 nm).

The proposed device achieved an SS value of 39.7 mV/decade for the minimum SS point and an average SS value of 38.5 mV/decade for biomolecules with a dielectric constant (ID_Cavity) of 12. This suggests that the device may offer a superior alternative for detecting a range of biomolecules, including the SARS-CoV-2 virus [55], various proteins, and amino acids [56], particularly those influenced b y dielectric constant and charge properties. Table V presents a comparison of the values of I_{on}/I_{off}, and the length of the cavity, in relation to already existing devices.

IV. CONCLUSION

The research presents a highly sensitive biosensor utilizing the dual cavity dielectric modulated ferroelectric charge plasma Tunnel FET (FE-CP-TFET). The creation of cavity regions at the source gate dielectric interfaces aims to enhance sensitivity by achieving a steeper edge at the source-channel junction. A comparative analysis between two structural variants, one with a cavity height of h_c = 2 nm and the other with h_c = 4 nm, is conducted to optimize the detection of bio-analytes. Employing the charge plasma technique helps mitigate negative conduction and improve random dopant fluctuations (RDF). F urthermore, i ntegration o f t he negative capacitance (NC) effect enhances low-power operation for detecting target biomolecules. The study includes sensitivity analyses, evaluating drain current, I_{ON}/I_{OFF} ratio, electric field, and transconductance, alongside linearity analysis. The impact of neutral and charged biomolecules trapped within the cavity region on these metrics is assessed. Notably, maximum drain current sensitivity reaches 2.76 x10^8, EF sensitivity is reported as 2.5, I_{ON}/I_{OFF} sensitivity stands at 1.45 x 10^7 with h_c = 4 nm for K = 8 at V_{GS} = 1 V. Linearity analysis, measured by I_{ON}/I_{OFF} fitness, a chieves a d egree o f r ^{2} ¿ 0 .8. T he findings suggest the reported biosensor holds promise for future biosensing applications.

REFERENCES

[1] B. J. Schaertel and R. Firstenbergeden, “Biosensors in the food industry: Present and future,” J. Food Protection, vol. 51, no. 10, pp. 811–820, Oct. 1988.
[2] G. Marrazza et al., “Disposable DNA electrochemical sensor for hybridization detection,” Biosensors Bioelectron., vol. 14, no. 1,pp. 43–51, Jan. 1999.
[3] T. G. Drummond, M. G. Hill, and J. K. Barton, “Electrochemical DNA sensors,” Nature Biotechnol., vol. 21, no. 10, pp. 1192–1199, Oct. 2003.
[4] M. Barbaro, A. Bonfiglio, and L. Raffo, “A charge-modulated FET for detection of biomolecular processes: Conception, modeling, and simulation,” IEEE Trans. Electron Devices, vol. 53, no. 1, pp. 158–166, Jan. 2006.
[5] Q. Zhang, W. Zhao, and A. Seabaugh, “Low-subthreshold-swing tunnel transistors,” IEEE Electron Device Lett., vol. 27, no. 4, pp. 297–300, Apr. 2006.
[6] P. C. Adell, H. J. Barnaby, R. D. Schrimpf, and B. Vermeire, “Band-to band tunneling (BBT) induced leakage current enhancement in irradiated fully depleted SOI devices,” IEEE Trans. Nucl. Sci., vol. 54, no. 6, pp. 2174–2180, Dec. 2007.
[7] H, Huang XJ, Gu B, Choi YK. “A dielectric-modulated field-effect transistor for biosensing. Nat Nanotechnol”. 2007 Jul;2(7):430-4. doi: 10.1038/nnano.2007.180. Epub 2007 Jun 24. PMID: 18654328.
[8] K. Boucart and A. M. Ionescu, “Double-gate tunnel FET with high K gate dielectric,” IEEE Trans. Electron Devices, vol. 54, no. 7, pp. 1725–1733, Jul. 2007.
[9] C.-H. Kim, C. Jung, H. G. Park, and Y.-K. Choi, “Novel dielectric modulated field-effect transistor for label-free DNA detection,” Biochip J., vol. 2, no. 2, pp. 127–134, 2008.
[10] D.-Y. Jang, Y.-P. Kim, H.-S. Kim, S.-H. K. Park, S.-Y. Choi, and Y.-K. Choi, “Sublithographic vertical gold nanogap for label-free elec trical detection of protein-ligand binding,” J. Vac. Sci. Technol. B, Microelectron. Process. Phenom., vol. 25, no. 2, pp. 443–447, 2007.
[11] S. O. Koswatta, M. S. Lundstrom, and D. E. Nikonov, “Perfor mance comparison between p-i-n tunneling transistors and conventional MOSFETs,” IEEE Trans. Electron Devices, vol. 56, no. 3, pp. 456–465, Mar. 2009, doi: 10.1109/TED.2008.2011934.
[12] C. Sandow, J. Knoch, C. Urban, Q.-T. Zhao, and S. Mantl, “Impact of electrostatics and doping concentration on the performance of silicon tunnel field-effect transistors,” Solid-State Electron., vol. 53, no. 10, pp. 1126–1129, Oct. 2009.
[13] X. Chen et al., “Electrical nanogap devices for biosensing,” Mater. Today, vol. 13, no. 11, pp. 28–41, Nov. 2010.
[14] A. M. Ionescu, L. Lattanzio, G. A. Salvatore, L. Michielis, K. Boucart, and D. Bouvet, “The hysteretic ferroelectric tunnel FET,” IEEE Trans. Electron Devices, vol. 57, no. 12, pp. 3518–3524, Dec. 2010.
[15] S. Agarwal, G. Klimeck, and M. Luisier, “Leakage-reduction design concepts for low-power vertical tunneling field-effect transistors,” IEEE Electron Device Lett., vol. 31, no. 6, pp. 621–623, Jun. 2010.
[16] S. Saurabh and M. J. Kumar, “Novel attributes of a dual material gate nanoscale tunnel field-effect transistor,” IEEE Trans. Electron Devices, vol. 58, no. 2, pp. 404–410, Feb. 2011.
[17] H. K. Chang et al., “Rapid, label-free, electrical whole blood bioassay based on nano biosensor systems,” ACS Nano, vol. 5, no. 12, pp. 9883–9891, Dec. 2011
[18] A. M. Ionescu and H. Riel, “Tunnel field-effect transistors as energy efficient electronic switches,” Nature, vol. 479, no. 7373, pp. 329–337, Nov. 2011.
[19] D. Sarkar and K. Banerjee, “Proposal for tunnel-field-effect-transistor as ultra-sensitive and label-free biosensors,” Appl. Phys. Lett., vol. 100, no. 14, Apr. 2012, Art. no. 143108.
[20] A. Hraziia, A. Vladimirescu, A. Amara, and C. Anghel, “An analysis on the ambipolar current in Si double-gate tunnel FETs,” Solid-State Electron., vol. 70, pp. 67–72, Apr. 2012.
[21] M. J. Kumar and S. Janardhanan, “Doping-less tunnel field effect transistor: Design and investigation,” IEEE Trans. Electron Devices, vol. 60, no. 10, pp. 3285–3290, Oct. 2013.
[22] D. Sarkar, W. Liu, X. Xie, A. C. Anselmo, S. Mitragotri, and K. Banerjee, “MoS2 field-effect transistor for next-generation label-free biosensors,” ACS Nano, vol. 8, no. 4, pp. 3992–4003, Apr. 2014, doi: 10.1021/nn5009148.
[23] S. Clima et al., “Identification of the ferroelectric switching process and dopant dependent switching properties in orthorhombic HfO_2: A first principles insight,” Appl. Phys. Lett. vol. 104, Mar. 2014, Art. no. 092906.

International Journal of Engineering Research & Technology (IJERT)
ISSN: 2278-0181
Vol. 14 Issue 04, April-2025

[24] S. Singh, P. Pal, and P. N. Kondekar, "Charge-plasma-based super-steep negative capacitance junctionless tunnel field effect transistor: Design and performance," Electron. Lett., vol. 50, no. 25, pp. 1963–1965, 2014.
[25] R. Vishnoi and M. Kumar, "Compact analytical drain current model of gate-all-around nanowire tunneling FET," IEEE Trans. Electron Devices, vol. 61, no. 7, pp. 2599–2603, Jul. 2014.
[26] M. Kumar and S. Jit, "A novel four-terminal ferroelectric tunnel FET for quasi-ideal switch," IEEE Trans. Nanotechnol., vol. 14, no. 4, pp. 600–602, Jul. 2015.
[27] J. Min, J. Wu, and Y. Taur, "Analysis of source doping effect in tunnel FETs with staggered bandgap," IEEE Electron Device Lett., vol. 36, no. 10, pp. 1094–1096, Oct. 2015.
[28] Singh, Deepika & Pandey, Sunil & Nigam, Kaushal & Sharma, Vaidhshiromani.Dheeraj & Yadav, Dharmendra & Kondekar, Pravin. (2016). A Charge-Plasma-Based Dielectric-Modulated Junctionless TFET for Biosensor Label-Free Detection. IEEE Transactions on Electron Devices. PP. 10.1109/TED.2016.2622403.
[29] S. Singh, P. N. Kondekar, and N. K. Jaiswal, "Label-free biosensor using nanogap embedded dielectric modulated Schottky tunneling source impact ionization MOS," Microelectron. Eng., vol. 149, pp. 129–134, Jan. 2016.
[30] S. Kanungo, S. Chattopadhyay, P. S. Gupta, K. Sinha, and H. Rahaman, "Study and analysis of the effects of SiGe source and pocket-doped channel on sensing performance of dielectrically modulated tunnel FET-based biosensors," IEEE Trans. Electron Devices, vol. 63, no. 6, pp. 2589–2596, Jun. 2016, doi: 10.1109/TED.2016.2556081.
[31] B. R. Raad, D. Sharma, K. Nigam, and P. Kondekar, "Physics-based simulation study of high-performance gallium arsenide phosphide indium gallium arsenide tunnel field-effect transistor," Micro Nano Lett., vol. 11, no. 7, pp. 366–368, Jul. 2016.
[32] B. R. Raad, K. Nigam, D. Sharma, and P. N. Kondekar, "Performance investigation of bandgap, gate material work function and gate dielectric engineered TFET with device reliability improvement," Superlattices Microstruct., vol. 94, pp. 138–146, Jun. 2016.
[33] A. Saeidi, A. Biswas, and A. M. Ionescu, "Modeling and simulation of low power ferroelectric non-volatile memory tunnel field effect transistors using silicon-doped hafnium oxide as gate dielectric," Solid State Electron., vol. 124, pp. 16–23, Oct. 2016.
[34] A. Saeidi, F. Jazaeri, I. Stolichnov, and A. M. Ionescu, "Double-gate negative-capacitance MOSFET with PZT gate-stack on ultra-thin body SOI: An experimentally calibrated simulation study of device performance," IEEE Trans. Electron Devices, vol. 63, no. 12, pp. 4678–4684, Dec. 2016.
[35] Device Simulation Software, Santa Clara, CA, USA: ATLAS Silvaco, 2016.
[36] M. Verma, S. Tirkey, S. Yadav, D. Sharma, and D. S. Yadav,"Performance assessment of a novel vertical dielectrically modulated TFET-based biosensor," IEEE Trans. Electron Devices, vol. 64, no. 9, pp. 3841–3848, Sep. 2017, doi: 10.1109/TED.2017.2732820.
[37] V. Nabaei, R. Chandrawati, and H. Heidari, "Magnetic biosensors: Modelling and simulation," Biosensors Bioelectron., vol. 103, pp. 69–86, Apr. 2017.
[38] V.-T. Nguyen, Y. S. Kwon, and M. B. Gu, "Aptamer-based environ mental biosensors for small molecule contaminants," Current Opinion Biotechnol., vol. 45, pp. 15–23, Jun. 2017.
[39] P. Dwivedi and A. Kranti, "Applicability of transconductance-to-current ratio (gm/ids) as a sensing metric for tunnel FET biosensors," IEEE Sensors J., vol. 17, no. 4, pp. 1030–1036, Feb. 15, 2017.
[40] D. Singh, S. Pandey, K. Nigam, D. Sharma, D. S. Yadav, and P. Kondekar, "A charge-plasma-based dielectric-modulated junctionless TFET for biosensor label-free detection," IEEE Trans. Electron Devices, vol. 67, no. 1, pp. 271–278, Jan. 2017.
[41] S. Singh and P. N. Kondekar, "Circuit performance and sensitivity analy sis of charge plasma based super-steep negative capacitance junctionless tunnel field effect transistor," J. Nanoelectron. Optoelectron., vol. 12, no. 5, pp. 442–451, May 2017.
[42] P. Venkatesh, K. Nigam, S. Pandey, D. Sharma, and P. N. Kondekar, "A dielectrically modulated electrically doped tunnel FET for appli cation of label free biosensor," Superlattices Microstruct., vol. 109, pp. 470–479, Sep. 2017.
[43] D. Sharma, D. Singh, S. Pandey, S. Yadav, and P. N. Kondekar, "Com parative analysis of full-gate and short-gate dielectric modulated electrically doped tunnel-FET based biosensors," Superlattices Microstruct., vol. 111, pp. 767–775, Nov. 2017.
[44] M. Verma, S. Tirkey, S. Yadav, D. Sharma, and D. S. Yadav, "Performance assessment of a novel vertical dielectrically modulated TFET based
[45] G. Wadhwa and B. Raj, "Parametric Variation Analysis of Symmetric Double Gate Charge Plasma JLTFET for Biosensor Application," in IEEE Sensors Journal, vol. 18, no. 15, pp. 6070-6077, 1 Aug.1, 2018, doi:10.1109/JSEN.2018.2846409.
[46] G. Wadhwa and B. Raj, "Parametric variation analysis of symmetric double gate charge plasma JLTFET for biosensor application," IEEE Sensors J., vol. 18, no. 15, pp. 6070–6077, Aug. 2018.
[47] A. Bhattacharyya, M. Chanda, and D. De, "Performance assessment of new dual-pocket vertical heterostructure tunnel FET-based biosensor considering steric hindrance issue," IEEE Trans. Electron Devices, vol. 66, no. 9, pp. 3988–3993, Sep. 2019.
[48] D. Kwon et al., "Negative capacitance FET with 1.8-nm-thick Zr-doped HfO_2 oxide," IEEE Electron Device Lett., vol. 40, no. 6, pp. 993–996, Jun. 2019.
[49] S. Kalra, M. J. Kumar, and A. Dhawan, "Reconfigurable FET biosensor for a wide detection range and electrostatically tunable sensing response," IEEE Sensors J., vol. 20, no. 5, pp. 2261–2269, Mar. 2020
[50] S. Ghosh, A. Chattopadhyay, and S. Tewari, "Optimization of heterogate-dielectric tunnel FET for label-free detection and identification of biomolecules," IEEE Trans. Electron Devices, vol. 67, no. 5, pp. 2157–2164, May 2020, doi: 10.1109/TED.2020.2978499.
[51] A. Anam, S. Anand, and S. I. Amin, "Design and performance analysis of tunnel field effect transistor with buried strained Si1-x Gex source structure-based biosensor for sensitivity enhancement," IEEE Sensors J., vol. 20, no. 22, pp. 13178–13185, Nov. 2020.
[52] V. D. Wangkheirakpam, B. Bhowmick, and P. D. Pukhrambam, "N+ pocket doped vertical TFET based dielectric-modulated biosensor con sidering non-ideal hybridization issue: A simulation study," IEEE Trans. Nanotechnol., vol. 19, pp. 156–162, 2020.
[53] S. Singh, A. K. S. Chauhan, G. Joshi, and J. Singh, "Design and investigation of SiGe heterojunction-based charge plasma vertical TFET for biosensing application," in Proc. Silicon, pp. 1–12, 2021.
[54] M. Patil, A. Gedam, and G. P. Mishra, "Performance assessment of a cavity on source charge plasma TFET-based biosensor," IEEE Sensors J., vol. 21, no. 3, pp. 2526–2532, Feb. 2021.
[55] A. Kaity, S. Singh, and P. N. Kondekar, "Silicon-on-nothing electro statically doped junctionless tunnel field effect transistor (SON-ED JLTFET): A short channel effect resilient design," Silicon, vol. 13, no. 1, pp. 9–23, Jan. 2021.
[56] H. Bharadwaj, N. Kumar, S. I. Amin, and S. Anand, "Charge plasma based vertical nanowire tunnel field effect transistor: Design and sensitivity analysis for biosensing application," Silicon, pp. 1–8, Nov. 2021
[57] Biswas, A., Rajan, C. & Samajdar, D.P. Sensitivity Analysis of Physically Doped, Charge Plasma and Electrically Doped TFET Biosensors. *Silicon* **14**, 6895–6908 (2022). https://doi.org/10.1007/s12633-021-01461-1
[58] K. N. Priyadarshani, S. Singh, and M. K. A. Mohammed, "Gate all-around junction less FET based label-free dielectric/charge modulation detection of SARS-CoV-2 virus," RSC Adv., vol. 12, no. 15, pp. 9202–9209, 2022.
[59] Sravani S.S., Balaji B., Srinivasa Rao K,"Qualitative Analysis of DG-TFET Structures with Gate material Engineering" Journal of Integrated Circuits and Systems 2022 DOI:10.29292/jics.v17i3.635.
[60] Balaji B., Srinivasa Rao K., Girija Sravani K., B K., Bindu Madhav N.V., Chandrahas K., Jaswanth B..Improved Drain Current Characteristics of HfO_2/SiO_2 Dual Material Dual Gate Extension on Drain Side-TFET.2023 Silicon.10.1007/s12633-022-01955-6